ELSEVIER

Fire Safety Journal **30** (1998) 333–356

Printed in Great Britain
0379–7112/98/$19.00

PII: S0379–7112 (97) 00050–7

On the Flight Paths of Metal Particles and Embers Generated by Power Lines in High Winds—a Potential Source of Wildland Fires

Stephen D. Tse & A. Carlos Fernandez-Pello*

Department of Mechanical Engineering, University of California at Berkeley, Berkeley, CA 94720, U.S.A.

(Received 20 November 1996; revised version received 14 July 1997; accepted 17 July 1997)

ABSTRACT

In dry grasslands, dangerous wildfires are of particular concern during hot, dry seasons in regions encountering high winds. It is possible that such winds can cause power cables to come close enough together to arc or collide with trees, and produce metal sparks or burning embers which can be carried by the wind and land in adjacent areas of dry vegetation. A major issue is whether or not such possibly generated particles can initiate a brush or grass fire. In this work, a predictive, numerical model is used to calculate trajectories, combustion rates, and lifetimes of metal particles and burning embers of different sizes for various wind conditions and terrain. Three distinct cases are studied: (1) hot particles produced by arcing copper power lines; (2) burning sparks produced by arcing aluminum power lines; and (3) burning embers produced by the collision of high voltage power lines with surrounding trees. The results show that for the same wind conditions, the distances reached by firebrands are the greatest, followed by aluminum and copper. Large aluminum sparks (e.g. 1·5 mm diameter) that do not burn up in flight travel farther than copper particles of the same size. Since copper particles do not emerge burning, they immediately cool down in flight, as they are carried away by the wind. Nonetheless, with a slightly larger heat capacity than that of aluminum (and non-regressing size), a copper particle can bring with it a significant amount of heat into its area of impact. Although smaller aluminum particles can burn out while in flight, larger aluminum particles can land while still burning. Burning embers or firebrands burn heterogeneously and are not susceptible to high Re extinction due to flame blow-off. Larger embers can land still burning; however, they may carry less heat than their metal counterparts. © *1998 Elsevier Science Ltd. All rights reserved.*

* Author to whom correspondence should be addressed.

NOTATION

A_{proj}	Projected area
c	Specific heat capacity
C_{D}	Drag coefficient
d	Diameter
$\vec{\mathbf{F}}$	Force vector
$\vec{\mathbf{g}}$	Gravity vector
$\bar{h}$	Average convection heat transfer coefficient
H	Height from ground of initial particle position
k	Thermal conductivity
K^0	Burning constant in a quiescent atmosphere (aluminum)
K	Modified burning constant for forced flow (aluminum)
l	Vertical distance from the ground
l_0	Roughness length
L	Horizontal distance traveled by particle
m	Mass
$\overline{Nu}$	Average Nusselt number
Pr	Prandtl number
$\dot{q}''$	Heat flux
$\vec{\mathbf{r}}$	Position vector
Re	Reynolds number
S	Surface area
Sc	Schmidt
t	Time
t_0	Ignition time
T	Temperature
$\mathscr{V}$	Volume
V_*	Friction velocity
$\vec{\mathbf{V}}$	Velocity vector
x	x-horizontal coordinate
y	y-horizontal coordinate
z	z-vertical coordinate

Greek

β^0	Burning constant in a quiescent atmosphere (firebrand)
β	Modified burning constant for forced flow (firebrand)
ϵ	Emissivity
κ	Von Kármán constant for turbulent flow
ρ	Density

σ Stefan–Boltzmann constant
ν Kinematic viscosity

Subscripts

air Air
c Critical
conv Convection
D Drag
eff Effective
g Gravity
l Liquid
P Particle
rad Radiation
R Resultant
W Wind
∞ Ambient

1 INTRODUCTION

In dry grasslands, dangerous wildfires are of concern, particularly during hot seasons experiencing high, dry winds. Such fires may be started by high winds that bring power lines close enough together that they arc and produce hot or burning (sparks) metal particles. These high temperature particles are then transported by the prevailing winds into bordering regions of dry vegetation. Another fire scenario involves power lines contacting trees to produce embers that are also carried by the wind into surrounding flora. Whether or not these metal particles and embers can initiate a fire depends on their energetic content, as well as the type of vegetation, at landing. The former depends on the initial formation state of the particle (i.e. size, temperature, density, etc.) and subsequent flight characteristics (i.e. thermo-aerodynamics, flight time, etc.). The latter depends on the nature (i.e. type, size, etc.) and state (i.e. moisture content, humidity, age, etc.) of the vegetation at the location of particle landing. Much interest exists in determining these issues in order to reduce the danger of wildland fires initiated in such a manner. The problem, however, is complex and, as seen above, involves a number of different issues. In this work, we only address the issue of particle characteristics during the flight path. The subject of ignition of vegetation is not treated.

To the best knowledge of the authors, the only work published related to the flight paths of metal particles generated by arcing cables is that of Mills and Hang.[1] The paper presents a fairly complete analysis of the problem for the case of aluminum cables, and discusses the difficulties in modeling the

problems and the limitations of the analysis. Although considerably more work has been done on the subject of flying embers,[2–6] these studies pertain to embers produced during an ongoing fire; and as such, the characteristics and trajectories of the embers are quite different than those of the present work. The embers of an ongoing fire are initially advected upward by the fire plume until eventually the prevalent winds drag them ahead of the fire. In addition, the size of such created embers can be much larger, and the distances reached much farther. Still, several of the subjects treated in these works are applicable to the present problem, and use of them will be made in the present analysis.

The characteristics of the present problem are as follows. When the cables come close enough to arc, the energy of the arc can cause some of the metal to melt and some to vaporize. The pressure from the gasified metal may be high enough to eject the molten metal as small particles, which are then carried away by the wind. The initial state of these particles depends on the energy of the arc and the type of metal of the conductor. The type of metal influences the problem due to its physical properties and combustion characteristics. In this work, we consider as potential conductors, copper and aluminum. Concerning the combustion of metals, Glassman[7,8] has proposed that for a metal to burn in the gaseous phase, the boiling point temperature of the oxide must be higher than that of the metal. If the oxide is more volatile than the metal, then only surface combustion is possible. Employing this criterion,[7,8] we find that since the boiling temperature of copper is higher than that of its oxides, copper can, at best, burn heterogeneously (as a surface reaction). Nonetheless, with a low heat of combustion, copper is not known to burn by itself in atmospheric air. Compared to copper, aluminum is less dense, has lower melting and boiling temperatures, and burns well in air[9–11] in the gas phase, concordant with the criterion of Glassman.[7,8] Another scenario involves the collision of high voltage power lines with neighboring trees. Under certain conditions, burning embers or firebrands may be produced. These burning embers can be carried by winds for longer distances due to their lower density and slower size-regression rate. Since these embers burn heterogeneously, high Reynolds numbers enhance their burning rate without extinction due to flame blow-off. However, they may carry less heat than their metal counterparts and are susceptible to larger cooling rates due to their higher emissivity.

2 THEORETICAL ANALYSES

2.1 Particle trajectories

2.1.1 *Equations of motion*

All particles, whether burning or not, in this analysis obey the same laws for their trajectory paths. Anchoring the coordinate axes on the initial position of

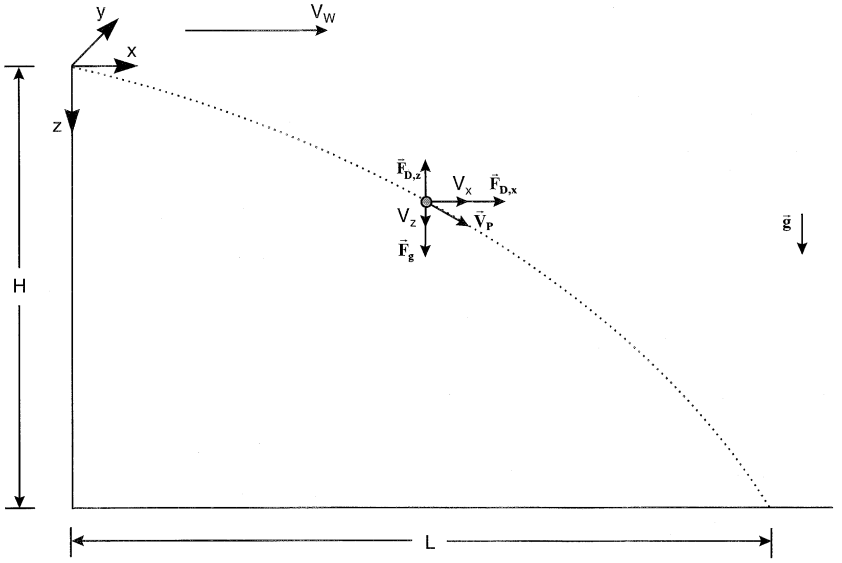

Fig. 1. Schematic of problem.

the particle, the trajectory model is presented in Fig. 1. Assuming that any gases ejected from a burning particle are distributed uniformly over the particle's surface and that any possible asymmetrical combustion produces only a very minor disturbance, the equation of motion for a Newtonian particle can be expressed as:

$$m_P \frac{d\vec{V}_P}{dt} = \vec{F}_g + \vec{F}_D, \tag{1}$$

$$\frac{d\vec{r}_P}{dt} = \vec{V}_P, \tag{2}$$

where $\vec{V}_P = [V_{P,x}, V_{P,y}, V_{P,z}]$ is the velocity of a particle, with respect to the ground; and $\vec{r}_P = [x_P, y_P, z_P]$ is the position of the particle. The buoyancy force on the particle is negligible because the density of a particle is much larger than that of the surrounding air. The gravity force is:

$$\vec{F}_g = m_P \vec{g} \tag{3}$$

where $\vec{g} = [0, 0, g]$. The drag force on a particle is

$$\vec{F}_D = \frac{1}{2} C_D \rho_{air} A_{proj} |\vec{V}_R|^2 \frac{\vec{V}_R}{|\vec{V}_R|}, \tag{4}$$

where $\vec{V}_R = \vec{V}_W - \vec{V}_P$ is the relative velocity between the particle and the air. The wind, $\vec{V}_W = [V_{W,x}, V_{W,y}, 0]$ is assumed to have only horizontal components, although its magnitude is a function of height above the ground, as will

be discussed in the following section. A_{proj} is the projected cross-sectional area of the particle. The drag coefficient C_{D} is a function of the Reynolds number, $Re = |\vec{\mathbf{V}}_{\text{R}}| \cdot d_{\text{P}}/\nu_{\text{air}}$. Properties, such as the kinematic viscosity ν_{air} and density ρ_{air} of air surrounding the particle, are evaluated at average conditions, which are taken to be the ambient pressure and the arithmetic mean of the flame/particle temperature and the ambient temperature. Although the bulk atmospheric flow may be turbulent due to frictional effects of the terrain, we assume that the physical turbulence scale is much much larger than the size of the particles in consideration; and consequently, the drag forces that the particles encounter are within the laminar regime. For generality, we assume that all particles are spherical in shape, which is a reasonable assumption for small metal droplets, since surface tension forces tend to maximize the volume to surface area ratios. Although burning embers can take on non-spherical shapes, they are also postulated to be spheres in this work. Nonetheless, the drag coefficients of various shapes are documented in the literature, and can easily be employed. For low to moderate values of Re, we invoke an empirically matched approximation for the drag coefficient of a smooth sphere:[12]

$$C_{\text{D}} = \frac{24}{Re}\left(1 + \frac{3Re}{16}\right)^{\frac{1}{2}} \quad \text{for } Re \leqslant 680. \tag{5}$$

[Note how eqn (5) approaches the Oseen approximation to Stoke's law of creeping flow for small Re.] For larger values of Re, we employ the laminar boundary layer approximation for the drag coefficient of a smooth sphere[12]:

$$C_{\text{D}} = 0.4 \quad \text{for } 680 \leqslant Re < 3 \times 10^5. \tag{6}$$

Possible reduction of drag due to surface ablation is not considered. Substituting the external forces [eqns (3) and (4)] on the spherical particle into eqn (1) and decomposing into x (horizontal), y (horizontal) and z (vertical) components gives:

$$\frac{\mathrm{d}V_{\text{P},x}}{\mathrm{d}t} = \frac{1}{2m_{\text{P}}} C_{\text{D}} \rho_{\text{air}} A_{\text{proj}} |\vec{\mathbf{V}}_{\text{R}}| (V_{\text{W},x} - V_{\text{P},x}), \tag{7}$$

$$\frac{\mathrm{d}V_{\text{P},y}}{\mathrm{d}t} = \frac{1}{2m_{\text{P}}} C_{\text{D}} \rho_{\text{air}} A_{\text{proj}} |\vec{\mathbf{V}}_{\text{R}}| (V_{\text{W},y} - V_{\text{P},y}), \tag{8}$$

$$\frac{\mathrm{d}V_{\text{P},z}}{\mathrm{d}t} = \frac{1}{2m_{\text{P}}} C_{\text{D}} \rho_{\text{air}} A_{\text{proj}} |\vec{\mathbf{V}}_{\text{R}}| V_{\text{P},z} - g \tag{9}$$

where:

$$\frac{dx_P}{dt} = V_{P,x}, \tag{10}$$

$$\frac{dy_P}{dt} = V_{P,y}, \tag{11}$$

$$\frac{dz_P}{dt} = V_{P,z}. \tag{12}$$

The solution of eqns (7)–(12) describes the particle trajectory path. If combustion is present, then the mass m_p of the particle and its diameter d_p are functions of the burning rate, as shown below. Also, the wind velocity profile depends on the type of terrain.

2.1.2 *Surface wind velocity distribution*

Since the terrain and roughness of the landscape influences the wind speed with respect to height above the ground, a description of the wind field should be included in the analysis to calculate the trajectories of the particles. Meteorological science reveals that there exists an atmospheric layer, called the friction layer, near the earth that reduces wind speeds, depending on the type of terrain. This reduction in wind is due to the frictional drag of the ground, extending up to a height of 1 km.[13] This frictional effect is due to eddy viscosity from turbulent whirling eddies, rather than to molecular viscosity alone, which only produces a laminar sub-layer less than a centimeter thick.[14] As wind blows over a rough landscape, it breaks into a series of irregular, twisting eddies—a process commonly referred to as mechanical turbulence. Within each eddy, the wind speed and direction fluctuate rapidly, producing irregular air motions known as wind gusts. Mechanical turbulence creates a drag on the flow of air far greater than that produced by molecular viscosity alone.[13]

Immediately adjacent to the earth's surface, within the large friction layer, there exists a region called the surface layer which is typically 30–50 m from the ground[14]—the region of interest in the present work. Modeling of the surface layer is straightforward because the vertical turbulent fluxes of momentum (Reynolds stresses) can be assumed constant with respect to height. A model which describes the general features of the flow field is presented below, it does not include the effects of buoyancy nor the effect of temperature stratification on the nature of turbulence in the surface layer. For a 'flat terrain' only horizontal wind components are needed, and the wind speed distribution within the surface layer can be well described by a logarithmic

profile:[14,15]

$$|\vec{\mathbf{V}}_{\mathrm{W}}| = \frac{V_*}{\kappa} \ln\left(\frac{l}{l_0}\right), \quad \text{for } l \geqslant l_0;$$

$$|\vec{\mathbf{V}}_{\mathrm{W}}| = 0, \text{ for } l < l_0. \tag{13}$$

where l is the distance from the ground, and the roughness length l_0 is a linear scale associated with the turbulent transport of shear stress; McRae et al.[16] gives roughness lengths for various surfaces as shown in Table 1. Von Kármán's constant κ is usually approximated to be $0 \cdot 4$. The friction velocity V_* is simply a characteristic wind speed constant that defines the wind speed, $|\vec{\mathbf{V}}_{\mathrm{W}}|$, to be a given value at some reference height (e.g. 10 m above the ground as in the Beaufort Scale)[17].

2.2 Copper particles

The literature shows that copper can burn at atmospheric pressure in pure oxygen,[18–21] or in air at elevated pressures[22]; however, to the best knowledge of the authors, no work documents self-sustained copper combustion in air at STP. The low heat of combustion (156 kJ/mol)[23] of copper in the presence of high heat losses by convection and radiation prevent copper from burning in air at STP. Thus, in the case of copper power lines, ejected particles most likely emerge molten but not burning. Immediately after creation, the copper particles cool down by convection and radiation as they are carried away by the wind. In this work, the copper particles are taken to be initially in the solid phase at the melting temperature (1083°C)[24]. The properties for copper used in this work are displayed in Table 2.

Assuming lumped capacitance for a particle, its temperature T_{P} is given by the solution of the transient energy equation:

$$(\rho \mathscr{V} c)_{\mathrm{P}} \frac{\mathrm{d}T_{\mathrm{P}}}{\mathrm{d}t} = -S_{\mathrm{P}}(\dot{q}''_{\mathrm{conv}} + \dot{q}''_{\mathrm{rad}}), \tag{14}$$

where ρ, $\mathscr{V}$, c are, respectively, the density, volume and specific heat capacity of the particle; S_{P} is the surface area of the particle; and $\dot{q}''_{\mathrm{conv}}$ and $\dot{q}''_{\mathrm{rad}}$ are, respectively, the convective and radiative heat fluxes lost by the particle to the surroundings.

The convective heat flux $\dot{q}''_{\mathrm{conv}}$ lost by a hot particle to an air stream is given by Newton's law of cooling:

$$\dot{\mathrm{q}}''_{\mathrm{conv}} = \bar{h} \cdot (T_{\mathrm{P}} - T_\infty), \tag{15}$$

where T_{P} and T_∞ are the temperatures of the particle and the ambient, respectively. The average convection heat transfer coefficient $\bar{h}$ is calculated

TABLE 1
Roughness lengths for various surfaces[a]

Surface	z_0 (m)
Very smooth (ice, mud flats)	10^{-5}
Snow	10^{-3}
Smooth sea	10^{-3}
Level desert	10^{-3}
Lawn	10^{-2}
Uncut grass	0·05
Fully grown root crops	0·1
Tree covered	1
Low-density residential	2
Central business district	5–10

[a] McRae et al.[16].

TABLE 2
Copper properties

Property	Value
Molecular weight	63·54 g/mol
Melting point[a]	1083°C
Boiling point[b]	2582°C
Density (at 300K)[c]	8933 kg/m^3
Specific heat, solid, 0 to t (°C)[a]	$0{\cdot}092 + 0{\cdot}000025t$ cal/(g K)
Specific heat, liquid[a]	0·112 cal/(g K)
Latent heat of fusion[b]	13 kJ/mole
Latent heat of vaporization[b]	305·1 kJ/mole
Heat of oxidation Cu_2O[a]	1·4 kJ/g of Cu
Heat of oxidation CuO[a]	2·543 kJ/g of Cu
Ignition temperature[d]	1027°C
Adiabatic combustion temperature (1 atm oxygen)[e]	927°C
Oxide melting point (Cu_2O)[b]	1235°C
Oxide melting point (CuO)[b]	1326°C
Oxide boiling point (Cu_2O)[b]	1800°C
Emissivity (stably oxidized at 600 K)[c]	0·5

[a] Butts (ed.)[24].
[b] White[51].
[c] Incropera and DeWitt[50].
[d] Clark and Hust[52].
[e] Grosse and Conway[18].

through the Nusselt number $\overline{Nu} = \bar{h}\mathrm{d_P}/k_{\mathrm{air}}$. For convective heat transfer relating to a solid sphere, we employ the correlation of Ranz and Marshall[25] for the average Nusselt number $\overline{Nu}$:

$$\overline{Nu} = 2 + 0{\cdot}6Re^{1/2}Pr^{1/3}. \tag{16}$$

The net radiative heat flux $\dot{q}''_{\text{rad}}$ lost by a hot particle to its surrounds is given by the Stefan–Boltzmann law:

$$\dot{q}''_{\text{rad}} = \sigma\varepsilon\cdot(T_{\text{P}}^4 - T_\infty^4), \tag{17}$$

where σ is the Stefan–Boltzmann constant; and ε is the emissivity of the particle.

Substituting the convective and radiative heat fluxes [eqns (15) and (17)] into eqn (14) for a spherical particle, the time rate of change of temperature can be solved to obtain:

$$\frac{\mathrm{d}T_{\text{P}}}{\mathrm{d}t} = -\frac{6}{(\rho\mathscr{V}c)_{\text{P}}d_{\text{P}}}(\bar{h}\cdot(T_{\text{P}} - T_\infty) + \sigma\varepsilon\cdot(T_{\text{P}}^4 - T_\infty^4)) \tag{18}$$

2.3 Aluminum particles

In the case of aluminum sparks, the ignition temperature is about 2054°C,[19] which corresponds to the melting point of its oxide. The criterion of Glassman[7,8] prescribes that aluminum burns in the vapor phase, due to the lower boiling point of the metal compared to its oxide. However, the accumulation of solid oxide on the droplet surface may inhibit ignition and combustion. Yet, if the spark is ejected with its oxide molten, aerodynamic forces can strip away the oxide layer to expose bare metal, allowing it to ignite and burn as a spherical liquid droplet. Some authors have argued that combustion of aluminum particles is actually much more complicated than that of other metals, such as magnesium, where the combustion reaction occurs in the gas phase, forming a spherical diffusion flame around the fuel droplet. For example, Fassel et al.[26] reported the formation of a hollow bubble of aluminum oxide surrounding an aluminum particle. Bartlett et al.[10] proposed and treated a model of burning particles which assumes that the vapor from the boiling aluminum droplet inflates the bubble of molten aluminum oxide; and the burning rate is controlled by diffusion through the liquid bubble. However, many authors[27–29] questioned this theory and believe that the vapor-phase diffusion model of Brzustowski and Glassman[30] is more applicable. The experiments resulting in aluminum oxide bubbles were usually conducted with methane-oxygen flames as a heat source. The advocates of the vapor-phase model averred that these hollow oxide shells are formed due to the presence of hydrogen[31] by evolution of the dissolved permanent gas. In later works,[11,32–34] experiments of combustion of aluminum particles in hydrogen-free environments indicated that good approximate comparisons can be made on the basis of the *d*-square law. For this reason, in this work, for aluminum particle combustion, we employ the *d*-square law of droplet combustion, i.e.

that the square of the droplet diameter decreases linearly with time:

$$d_{l,0}^2 - d_l^2 = K^0(t - t_0), \tag{19}$$

where K^0 is the burning constant in a quiescent atmosphere and t_0 is the ignition time.

Wind will affect droplet burning by increasing its burning rate due to the enhancement of the heat transfer from the flame to the droplet. The analogy is that of the increase in convection heat transfer for a sphere due to the thinning of the boundary layer. For droplets burning in forced convection, Williams[35] shows that we can employ a modified burning constant:

$$K = K^0(1 + 0 \cdot 276Re^{1/2}Pr^{1/3}), \tag{20}$$

where K^0 is given by eqn (19) and Pr is the Prandtl number. The diameter of the steady-state burning droplet decreases as

$$\frac{\mathrm{d}(d_p^2)}{\mathrm{d}t} = -K. \tag{21}$$

Although radiation effects are not explicitly included in eqn (21), they are in general negligible[36] (at least when well within ignition and extinction limits). Nonetheless, some radiation effects are somewhat incorporated through the use of an experimental value for the burning constant K^0 of aluminum, which varies between $2{\cdot}4 \times 10^{-3}$ cm^2/s and $3{\cdot}2 \times 10^{-3}$ cm^2/s.[37] In this work, we employ an average value of $K^0 = 2{\cdot}8 \times 10^{-3}$ cm^2/s for the burning constant of aluminum. The aluminum particle surface is at approximately its boiling temperature (2480°C),[38] with its surrounding flame at the aluminum oxide boiling temperature (3527°C).[38] The properties for aluminum used in this work are shown in Table 3.

Depending upon the Reynolds number of the flow that the droplet encounters, it will either extinguish due to blow-off of the surrounding diffusion flame front, or burn until all of the metal is consumed or until it is quenched upon striking the ground. In early work, Spalding[39] observed that a flame envelops a burning sphere only for low values of the ratio of flow velocity to droplet diameter. With increasing flow velocities, the continuous envelope flame surrounding the droplet breaks up; and at a critical value of the velocity, the flame stabilizes only in the aerodynamic wake behind the droplet. Flame blow-off and extinction occurs when the flow time (ratio of droplet diameter to flow velocity) is of the same order as the characteristic reaction time[40]. Gallahalli and Brzustowski[41] found that the envelope flame is transformed into a wake flame at a critical Reynolds number, $Re_c = 138$, with Re evaluated at an average temperature of the flame and the ambient temperature. The burning rate decreases by over a factor of 3 when an envelope flame transforms into a wake flame[41]. Following these results, in this work, aluminum is

TABLE 3
Aluminum properties

Property	Value
Molecular weight	26·98 g/mol
Melting point[a]	660°C
Boiling point[a]	2480°C
Density (at 300K), solid[b]	2702 kg/m^3
Density, liquid[a]	2380 kg/m^3
Mean specific heat (0 to 658°C), solid[a]	1·045 kJ(kg K)
Latent heat of fusion[c]	10·67 kJ/mole
Latent heat of vaporization[c]	293·72 kJ/mole
Heat of combustion[a]	838 kJ/mole of Al
Ignition temperature[d]	2054°C
Adiabatic combustion temperature[d]	3732°C
Burning constant, K^{0}[e]	$2{\cdot}8 \times 10^{-3}$ cm^2/s
Oxide melting point (Al_2O_3)[a]	2045°C
Oxide boiling point (Al_2O_3)[a]	3527°C
Emissivity[f]	0·3

[a] King[38].
[b] Incropera and DeWitt[50].
[c] Emsley[53].
[d] Abbud-Madrid et al.[19].
[e] Wilson and Willians[37].
[f] Mills and Hang[1].

assumed to burn with an envelope flame for $Re < 138$; and eqn (21) is employed for the burning aluminum droplet. Extinction is assumed to occur at $Re \geqslant 138$; and the aluminum particle, which is considered to be initially at its boiling temperature, cools down due to convective and radiative heat transfer to the environment. The same heat transfer calculations as prescribed for copper particles are used. The latent heat of fusion for the change of phase, from liquid to solid, is included in the calculations. Possible reduction of mass due to stripping by shearing effects from the air flow[42] is not considered.

Flame extinction also occurs for a critical size of the diminishing droplet when the mass diffusion rate of fuel exceeds the burning rate in the diffusion flame-sheet.[43] However, since the critical diameter at which a droplet cannot develop a flame is very small (of the order of 5 μm),[43] an aluminum particle in this work is allowed to simply burn out.

2.4 Burning embers (firebrands)

High voltage power lines colliding with neighboring trees can, under certain conditions, produce burning embers or firebrands which can be carried by winds. These embers can burn heterogeneously (glowing combustion); and thus, high Reynolds numbers can enhance their burning rate without

extinction due to flame blow-off. On the other hand, the embers carry less heat than their metal counterparts and are susceptible to larger cooling rates due to their higher emissivity.

In firebrand combustion modeling, there is the additional difficulty that as the particle burns it loses mass and volume, but not in a manner which can be described solely by the d-square law of droplet combustion. Woody material is pyrolyzed by heat supplied by heterogeneous (glowing) combustion of the wood on the outer surface of the firebrand, as well as by homogeneous gas-phase oxidation of volatiles diffusing out of the firebrand.[44] The pyrolysis of the solid is a subsurface volumetric chemical process.[45] Consequently, the particle loses mass via both in-depth pyrolysis and surface combustion; and it loses volume only from the heterogeneous (glowing) combustion at the outer surface.

Tarifa et al.'s[46] experiments on the burning of wood spheres in forced convection remain to date the best available data on particle mass loss rate and size regression rate with relative wind velocity as a parameter. However, the authors[46] did not provide explicit expressions for the burning laws. Consequently, in this work, we have fit the mass loss rate and size regression rate of Tarifa et al.[46] based on some physical arguments and empirical data matching. Nusselt's shrinking drop theory[45] for a pyrolyzing solid predicts that the time-averaged mass loss rate is proportional to the initial diameter of the particle. In the model, the outer surface of the sphere is held at a constant temperature and a pyrolysis front propagates inward. The d-square law seems applicable to firebrand combustion, where heterogeneous reactions on the outer surface resemble the flame and a regressing effective mass diameter d_{eff} simulates the pyrolysis front. Also, the use of the modified burning constant, as in eqn (20), to account for wind effects seems appropriate since an increased burning rate due to a thinning boundary layer should also apply here. Employing the Frössling[47] relation for our calculations, the effective mass diameter d_{eff} decreases as:

$$\frac{\mathrm{d}(d_{\mathrm{eff}}^2)}{\mathrm{d}t} = -\beta, \tag{22}$$

where $\beta = \beta^0(1 + 0.276 Re^{1/2} Sc^{1/3})$; and the mass m_{P} of the particle at any given time is approximated by:

$$m_{\mathrm{P}} = \frac{\rho_{\mathrm{P},0} \pi d_{\mathrm{eff}}^3}{6}. \tag{23}$$

The burning rate constant β^0 is empirically fit to match the data of Tarifa et al.[46] Noteworthy, d_{eff} is not an absolute demarcation of the pyrolysis front because the particle mass expression of eqn (23) includes the mass of the

residual char, due to the fitting of Tarifa et al.'s[46] data. Nevertheless, since the density of the woody material is much larger than that of the char, d_{eff} can closely track the pyrolysis front. The Reynolds number Re is still determined using the actual particle diameter d_{P}, whose size regression rate is discussed below.

Although d_{eff} is regressing in a d-square law fashion, the actual diameter d_{P} of the particle is not, as shown in Tarifa et al.'s[46] data. Employing the same burning rate constant β^0 for the mass burning rate, we have been able to satisfactorily match Tarifa et al.'s[46] size regression data for the actual particle diameter d_{P} with the following expression:

$$d_{\text{P},0}^4 - d_{\text{P}}^4 = \chi\beta^2(t^2 - t_0^2), \tag{24}$$

where χ is determined to be $3^{1/2}$, for best data fitting. Note the similarity of eqn (24) with eqn (19); there may be some physical explanation for this resemblance, but at present, we only regard it as coincidence. Eqn (24) can be expressed in differential form as:

$$\frac{d(d_{\text{P}}^4)}{dt} = -2\sqrt{3}\beta^2 t, \tag{25}$$

Using eqns (23) and (25), we arrive at good agreement with Tarifa et al.'s[46] data for mass loss rate and size regression with air velocity as a parameter. For low air-flow velocities, $\beta^0 = 4{\cdot}3 \times 10^{-7}\ \text{m}^2/\text{s}$ allows a satisfactory fit of Tarifa et al.'s[46] data, as shown in Fig. 2(a); for high air-flow velocities, $\beta^0 = 5{\cdot}3 \times 10^{-7}\ \text{m}^2/\text{s}$ provides an excellent fit, as shown in Fig. 2(b). For our calculations, we utilize an average burning rate constant, $\beta^0 = 4.8 \times 10^{-7}\ \text{m}^2/\text{s}$, with a burning firebrand temperature of 993 K, as given by Ohlemiller's[48] experiments with smoldering wood in forced air flow. The properties for firebrands used in this work are shown in Table 4.

TABLE 4
Firebrand properties

Property	Value
Density, oak[a]	545 kg/m^3
Specific heat, wood[b]	1·466 kJ/(kg K)
Specific heat, char[b]	0·712 kJ/(kg K)
Surface combustion temperature[c]	720°C
Emissivity[d]	0·9
Burning rate constant, β^{0}[e]	$4{\cdot}8 \times 10^{-7}\ \text{m}^2/\text{s}$

[a] Incropera and DeWitt[50].
[b] Atreya[49].
[c] Ohlemiller[48].
[d] Siegel and Howell[54].
[e] Empirical fit of Tarifa's[46] data.

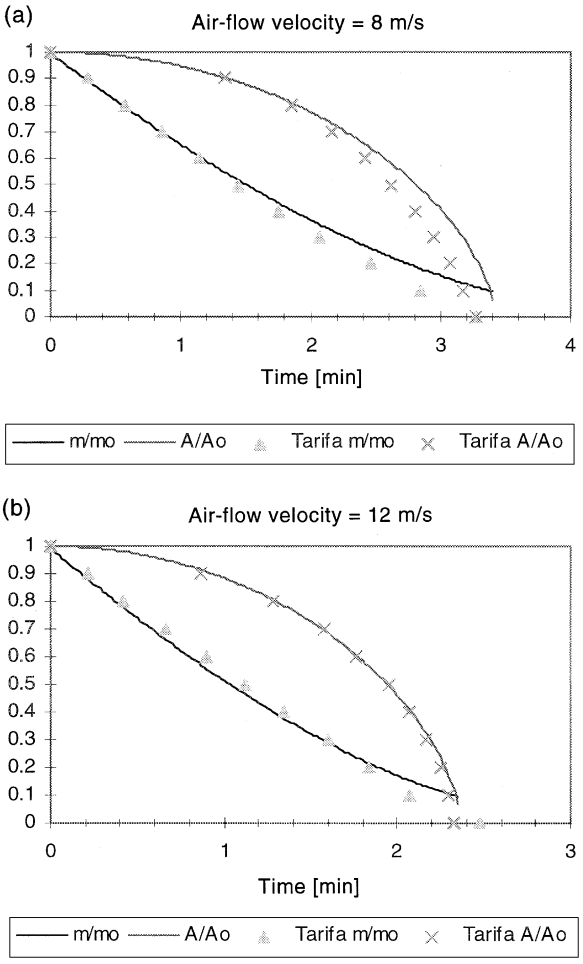

Fig. 2. Comparison of empirical fit with Tarifa et al.'s[46] data for mass loss rate and size regression for spherical firebrands of oak wood (m = mass, A = surface area). Initial particle diameter = 22 mm. For empirical fit: firebrand temperature assumed to be 993 K. (a) $\beta^0 = 4.3 \times 10^{-7}$ m^2/s for initial $Re < 3545$; (b) $\beta^0 = 5.3 \times 10^{-7}$ m^2/s for initial $Re \geqslant 3545$.

As a firebrand burns in its flight, it may eventually be reduced totally to char. The data of Tarifa et al.[46] allow for complete combustion of oak firebrands at high air velocities (>4 m/s); but the final char yield is $m/m_0 \approx 0{\cdot}16$ at low air velocities ($\sim$2 m/s). Atreya[49] gives a final char yield of $\rho/\rho_0 \approx 0{\cdot}24$ for maple and pine woods. In this work, heterogeneous combustion extinction is assumed to occur when $m/m_0 = 0{\cdot}24$. Upon extinction, the firebrand is assumed to cool down from an initial temperature of 993 K, according to the heat transfer processes discussed in the copper particles section.

3 RESULTS AND DISCUSSION

A computer code was written to solve the set of coupled ordinary differential equations [eqns (7)–(12), (18), (21), (22) and (25)] using a fourth order Runge–Kutta technique, for various initial particle sizes and wind speeds. Air properties as functions of temperature are determined from a power curve fit of empirical data[50] for thermophysical properties of air in the range of interest. The code allows for many parameters to be varied; however, the primary parameters of interest are particle diameter and wind speed. For all cases, a wind distribution for a flat terrain of uncut grass is applied. It is assumed that the power lines are at a height of 10 m above the ground.

3.1 Copper particles

We assume that copper particles are produced by arcing high-voltage power cables. This is a violent process which most likely ejects particles in various directions. In this work, an ejection speed of 1 m/s is employed for all cases, although a constant ejection momentum may be more appropriate since different diameter (and thus mass) particles are considered. Fig. 3 shows a hemispherical distribution of ejection angles of 1·5-mm-diameter copper particles for a single wind velocity of 48·3 km/h. As expected, a particle ejected at 45° above the horizon with the wind direction travels the farthest. This ejection angle is used for all copper particle trajectory paths shown in Fig. 4, which examines particles with diameters of 0·5 mm, 1 mm, 1·5 mm and 2 mm for a wind speed of 48·3 km/h. Since the copper particles are not ejected burning, they cool down along their flight path; and their temperatures are also displayed in Fig. 4. For a given wind speed, smaller diameter particles travel farther than larger ones. At the same time, however, smaller diameter

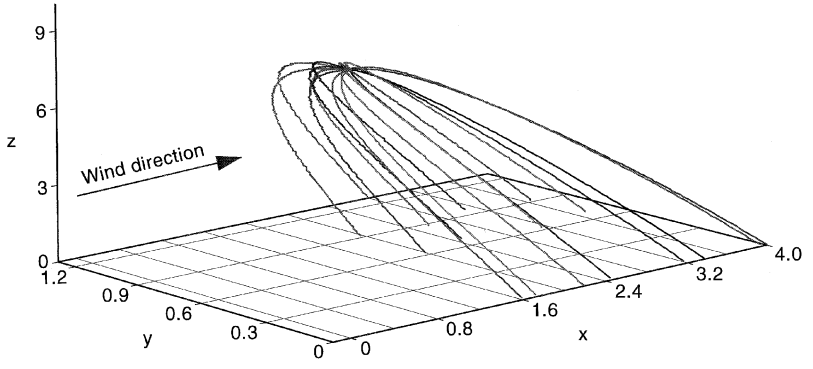

Fig. 3. Copper particle trajectories at various ejection angles, 1.5 mm diameter particles, 48.3 km/h wind speed.

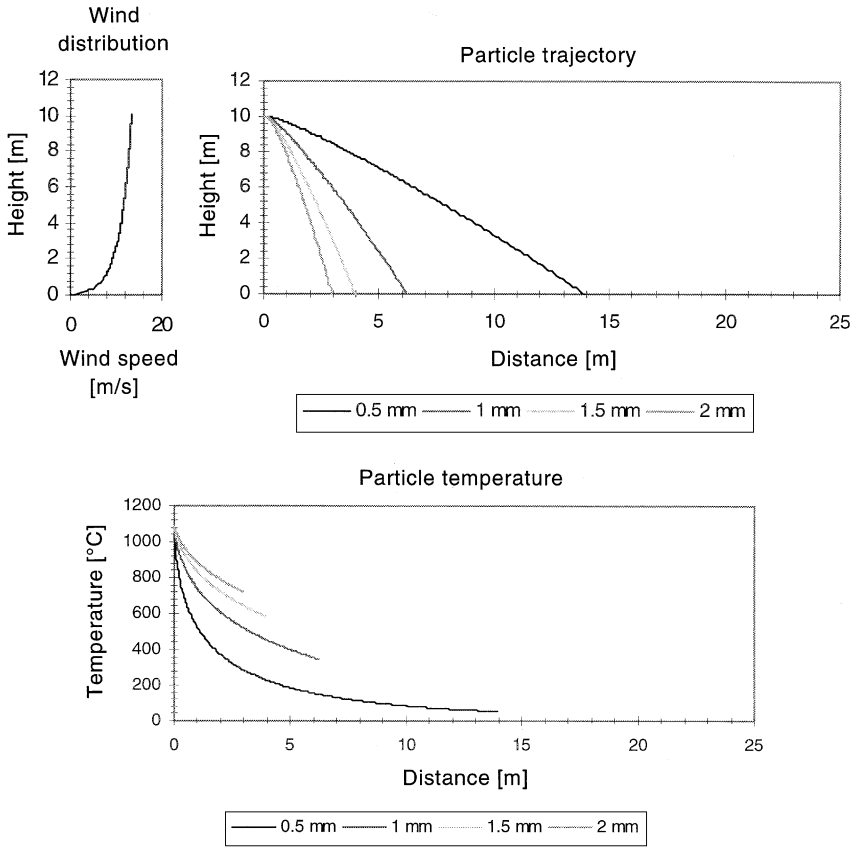

Fig. 4. Copper particle trajectories and temperature variation for various initial particle diameters, 48.3 km/h wind speed.

particles land with lower temperatures; and their smaller masses result in smaller total amounts of heat brought to locations of impact. As expected for a given size, particles land farther with increasing wind speeds.

3.2 Aluminum particles

As for the case of copper particles, aluminum particles are assumed to be ejected at a speed of 1 m/s. Fig. 5 shows a hemispherical distribution of ejection angles of 1·5-mm-diameter aluminum particles for a single wind velocity of 48·3 km/h. Although aluminum particles are ejected burning, the 1·5-mm-diameter particles of Fig. 5 do not burn out before impact (for a 48·3 mph wind speed); again, a particle ejected at 45° above the horizon with the wind direction travels the farthest. Similar to the copper particle cases, this

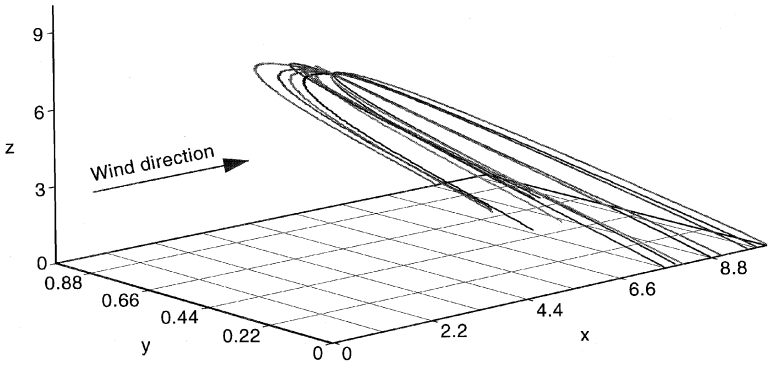

Fig. 5. Aluminum particle trajectories at various ejection angles, 1.5 mm diameter particles, 48.3 km/h wind speed.

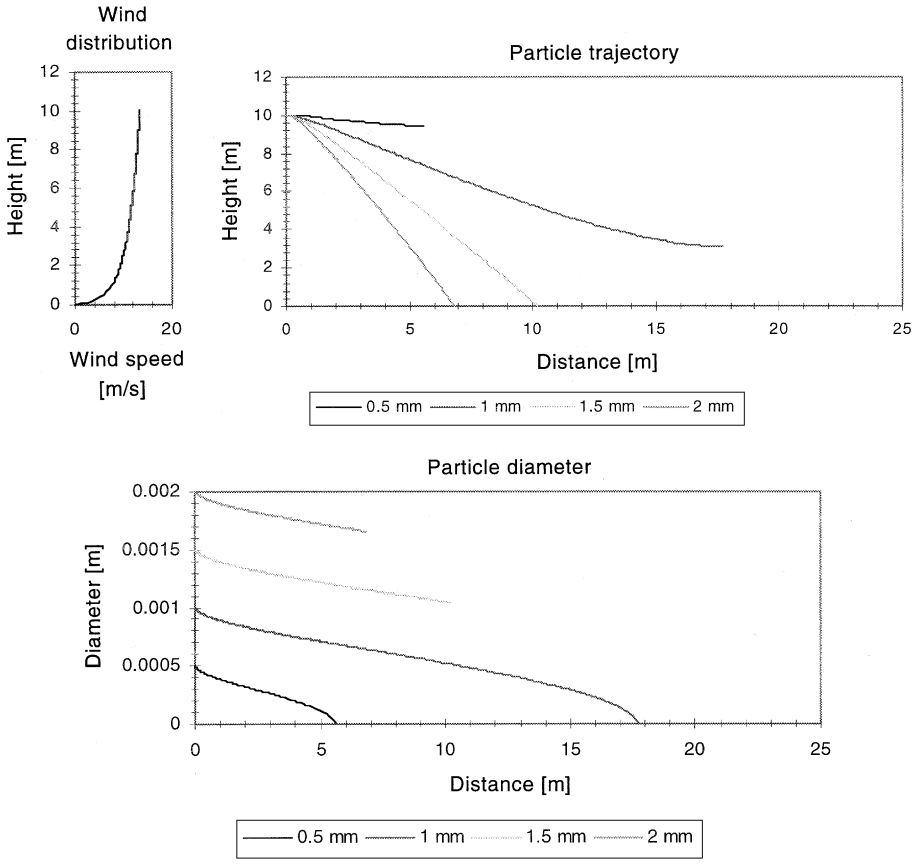

Fig. 6. Aluminum particle trajectories and diameter variation for various initial particle diameters, 48.3 km/h wind speed.

ejection angle is employed for all aluminum particle trajectory paths shown in Fig. 6, which examines particles with diameters of 0·5 mm, 1 mm, 1·5 mm and 2 mm for a wind speed of 48·3 km/h. Due to the low *Re* resulting from the high flame temperature of aluminum (high air viscosity), none of the burning particles extinguishes from flame blow-off for the wind speeds investigated. Consequently, all of the particles in Fig. 6 are at their boiling temperatures throughout their flight paths; and their temperatures are not plotted. Instead, since the diameters of the particles regress during burning, their diameters as a function of their horizontal distance traveled are displayed in Fig. 6. Although smaller particles can be carried farther than larger particles by the wind, smaller particles are also more likely to burn out along their trajectory path, as shown in Fig. 6; and only the larger particles reach the ground. For the burning particles that reach the ground, the smaller particles travel farther

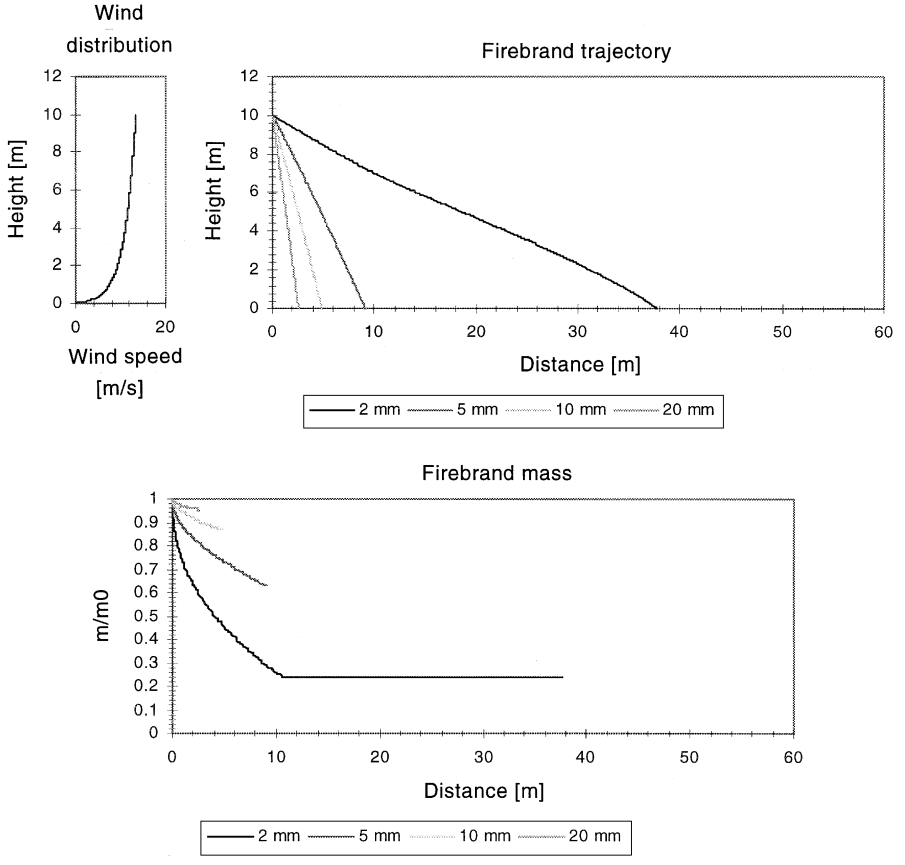

Fig. 7. Firebrand trajectory and mass variation for various initial firebrand diameters, 48.3 km/h wind speed.

horizontally, but also bring less total amounts of heat to their locations of impact. As expected, for particles of the same size that reach the ground, particles land farther with increasing wind speeds.

3.3 Burning embers (firebrands)

The burning embers or firebrands produced by high voltage power lines colliding with neighboring trees may also emerge with an initial velocity, however, since the process is probably less violent than that resulting from arcing, we assume in this work that burning embers are generated with no ejection velocity. In addition, the sizes of these particles are most likely larger than copper and aluminum particles. All firebrands are assumed to be initially burning, with extinction occurring when the mass to initial mass ratio goes below 0·24. Trajectory paths for firebrands with diameters of 2 mm, 5 mm, 10 mm and 20 mm for wind at a speed of 48.3 km/h are shown in Fig. 7. For the cases investigated, only the 2-mm-diameter firebrands extinguish and cool down; their temperatures as a function of horizontal distance traveled are shown in Fig. 8. For the wind speeds encountered, the 2-mm-diameter firebrands all cool down fast enough to land at ambient temperature. Firebrand diameter as a function of trajectory path is not plotted because it varies very little for all cases studied. Instead, firebrand mass as a function of horizontal distance is plotted alongside trajectory paths in Fig. 7. Larger firebrands land with a higher mass to initial mass ratio than smaller ones. Smaller firebrands travel farther than larger ones, but, like the copper and aluminum particles, also bring less total amounts of heat to their locations of impact. In addition, only larger particles are capable of landing burning.

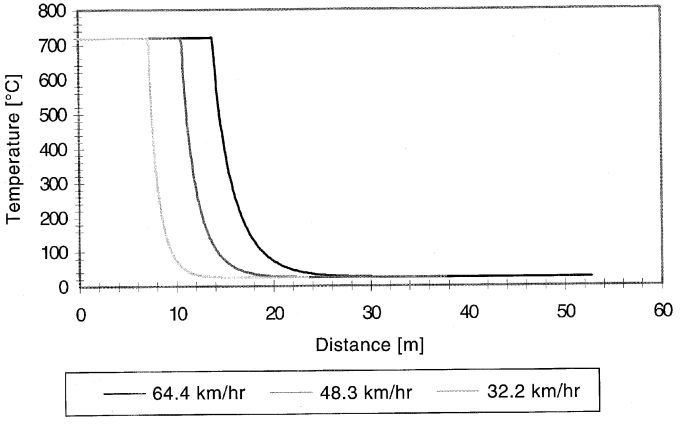

Fig. 8. Variation of the firebrand temperatures with the distance from ejection for several wind speeds, 2 mm diameter particles.

4 CONCLUDING REMARKS

This work shows that the distance reached by particles depends on many variables. Larger particles have larger projected areas for wind drag, but at the same time, more mass to be accelerated. Consequently, lower density particles, e.g. firebrands, with larger diameters can be carried for longer distances. Another factor is the temperature of the particle, since higher temperatures result in lower Re and larger C_D. Depending upon the size and temperature at which the particles hit the ground, they can present a fire danger. In the case of copper power lines, ejected particles most likely emerge molten but not burning, since copper hardly burns in atmospheric air. The copper particles will cool down as they are carried away by the wind, however, being three times denser than aluminum, their travel distance will be smaller than that of an aluminum particle of the same size. Nonetheless, with a slightly larger heat capacity than that of aluminum (and non-regressing size), a copper particle can bring a significant amount of heat with it into its area of impact. Large aluminum particles can land while still burning, however, smaller particles can burn out while in flight. In the third case, burning embers or firebrands can be carried by winds for long distances, due to their low density and slow size-regression rate, into regions far from their origin. Additionally, since these embers burn heterogeneously, high Re enhance their burning rate, without extinction due to flame blow-off, and can land still burning. At the same time, however, they may carry less heat than their metal counterparts and are susceptible to larger cooling rates due to their higher emissivity.

ACKNOWLEDGEMENTS

This work was partially supported by San Diego Gas and Electric; thanks are due to Mr C. L. Davis for his support to this project. The authors would also like to thank Professor J. L. Torero for his help during the initial work with aluminum particles, and Prof. T. C. Cheng and Mr R. A. Anthenien for their helpful discussions during the development of this work.

REFERENCES

1. Mills, A. F. & Hang, X., Trajectories of sparks from arcing aluminum power cables. *Fire Technology*, **20** (1984) 5–14.
2. Tarifa, C. S., Del Notario, P. P. & Moreno, F. G., On the flight paths and lifetimes of burning particles of wood. Tenth Symposium (International) on Combustion. The Combustion Institute, Pittsburgh, 1965 pp. 1021–37.
3. Lee, S. L. & Hellman, J. M., Firebrand trajectory study using an empirical velocity-dependent burning law. *Combustion and Flame*, **15** (1970) 265–74.

4. Muraszew, A., Fedele, J. B. & Kuby, W. C., Trajectory of firebrands in and out of fire whirls. *Combustion and Flame*, **30** (1997) 321–24.
5. Clements, H. B., Lift-off of forest firebrands. In USDA Forest Service Research Paper SE-159. Southeast Forest Experiment Station, Asheville, N. C., March 1977.
6. Albini, F. A., Transport of firebrands by line thermals. *Combustion Science and Technology*, **32** (1983) 277–88.
7. Glassman, I., Metal combustion processes. In ARS Preprint 938-59, November, 1959.
8. Glassman, I., Combustion of metals, physical considerations. In Solid Propellant Rocket Research, ed. M. Summerfied. Academic Press, New York, 1960.
9. Friedman, R. & Macek, A., Ignition and combustion of aluminium particles in hot ambient gases. *Combustion and Flame*, **6** (1962) 9–19.
10. Bartlett, R. W., Ong, J. N., Jr, Fassell, W. M., Jr & Papp, C. A., Estimating aluminium particle combustion kinetics. *Combustion and Flame*, **7** (1963) 227–34.
11. Macek, A., Fundamentals of combustion of single aluminum and beryllium particles. Eleventh Symposium (International) on Combustion. The Combustion Institute, Pittsburgh, 1967 pp. 203–17.
12. Kundu, P. K., Fluid Mechanics. Academic Press, San Diego, 1990.
13. Ahrens, D. C., Meteorology Today: An Introduction to Weather, Climate, and the Environment. West Publishing Company, St. Paul, 1985.
14. Seinfeld, J. H., Atmospheric Chemistry and Physics of Air Pollution. John Wiley, New York, 1986.
15. Sutton, O. G., Micrometeorology. McGraw-Hill, New York, 1953, p. 333.
16. McRae, G. J., Goodin, W. R. & Seinfeld, J. H., Development of a second-generation mathematical model for urban air pollution. I. Model formulation. *Atmos. Environ.*, **16** (1982) 679–96.
17. Moran, J. M., Morgan, M. D. & Pauley, P. M., Meteorology, The Atmosphere and the Science of Weather. MacMillan, New York, 1991.
18. Grosse, A. V. & Conway, J. B., Combustion of metals in oxygen. *Industrial and Engineering Chemistry*, **50**(4) (1958) 663–72.
19. Abbud-Madrid, A., Branch, M. C., Feiereisen, T. J. & Daily, J. W., Ignition of bulk metals by a continuous radiation source in a pure oxygen atmosphere. In Flammability and Sensitivity of Materials in Oxygen-Enriched Atmospheres, ASTM STP 1197, eds Dwight D. Janoff & Joel M. Stoltzfus. American Society for Testing and Materials, Philadelphia, 1993.
20. Abbud-Madrid, A., Fiechtner, G. J., Branch, M. C. & Daily, J. W., Ignition and combustion characteristics of bulk metals, normal-gravity test results. In 32nd Aerospace Sciences Meeting and Exhibit, Paper AIAA 94-0574. January, 1994.
21. Stoltzfus, J. M., Lowrie, R. & Gunaji, M. V., Burn propagation behavior of wire mesh made from several alloys. In Flammability and Sensitivity of Materials in Oxygen-enriched Atmospheres, Fifth Volume, ASTM STP 1111, 1991, pp. 326–37.
22. Reynolds, W. C., Investigation of Ignition Temperatures of Solid Metals, Technical Note D-182. NASA, Washington D. C., 1966.
23. Lide, D. R., Jr, Editor, JANAF Thermochemical Tables, 3rd edn, Vol. 14. American Chemical Society and American Institute of Physics, New York, 1985.

24. Butts, A., ed. Copper, The Science and Technology of the Metal, Its Alloys and Compounds. American Chemical Society Monograph Series, Reinhold, New York, 1954.
25. Ranz, W. & Marshall, W., Evaporation from drops. *Chem. Eng. Prog.*, **48** (1952) 141–146.
26. Fassell, W. M., Papp, C. A., Hildenbrand, D. L. & Sernka, R. P. The experimental nature of the combustion of metal powders. In Solid Propellant Rocket Research. Academic Press, New York, (1960) 259–70.
27. Brzustowski, T. A., Comments on the paper 'estimating aluminium particle combustion kinetics'. *Combustion and Flame*, **8** (1964) 339–340.
28. Drew, C. M., Some further comments on 'estimating aluminium particle combustion kinetics'. *Combustion and Flame*, **9** (1965) 205–208.
29. Prentice, J. L., On the combustion of single aluminium particles. *Combustion and Flame*, **9** (1965) 208–210.
30. Brzustowski, T. A. & Glassman, I., Vapor-phase diffusion flames in the combustion of magnesium and aluminum, I. Analytical developments. In Heterogeneous Combustion. Academic Press, New York, 1964, pp. 75–116.
31. Gordon, D. A., Solid Propellant Rocket Research. Academic Press, (1960) 271.
32. Friedman, R. & Macek, A., Combustion studies of single aluminum particles. Ninth Symposium (International) on Combustion. Academic Press, New York, (1963) 703–12.
33. Davis, A., Solid propellants: the combustion of particles of metal ingredients. *Combustion and Flame*, **7** (1963) 359.
34. Prentice, J. L., Drew, C. H. & Christensen, H. C., Preliminary studies of high-speed photography of aluminium particle combustion in flames. *Pyrodynamics*, **3** (1965) 81–90.
35. Williams, F. A., Combustion Theory. Addison-Wesley, Menlo Park, 1985.
36. Williams, A., Combustion of droplets of liquid fuels, a review. *Combustion and Flame*, **21** (1973) 1–31.
37. Wilson, R. P. & Williams, F. A., Experimental study of the combustion of single aluminum particles in O_2/Ar. Thirteenth Symposium (International) on Combustion. The Combustion Institute, Pittsburgh, 1971, pp. 833–45.
38. King, F., Aluminum and its Alloys. Ellis Horwood, Chichester, 1987.
39. Spalding, D. B., The combustion of liquid fuels. Fourth Symposium (International) on Combustion. The Williams and Wilkins Company, Baltimore, 1953, pp. 847–64.
40. Fernandez-Pello, A. C. & Law, C. K., On the mixed-convective flame structure in the stagnation point of a fuel particle. Nineteenth Symposium (International) on Combustion. The Combustion Institute, Pittsburgh, 1982, pp. 1037–44.
41. Gollahalli and Brzustowski, Experimental studies on the flame structure in the wake of a burning droplet. Fourteenth Symposium (International) on Combustion. The Combustion Institute, Pittsburgh, 1973, pp. 1333–43.
42. Gany, A. & Caveny, L. H., Mechanism of chemical and physical gas-metal interactions in very high shearing regimes. Nineteenth Symposium (International) on Combustion. The Combustion Institute, Pittsburgh, 1982, pp. 731–40.
43. Chomiak, J., Combustion, A Study in Theory, Fact, and Application. Gordon and Breach Science, New York, 1990, p. 202.
44. Albini, F. A., Spot fire distance from burning trees—A predictive model. USDA Forest Service, General Technical Report INT-56, July 1979.

45. Kanury, A. M., Introduction to Combustion Phenomena. Gordon and Breach Science, New York, 1975.
46. Tarifa, C. S., Del Notario, P. P., Moreno, F. G. & Villa, A. R., Transport and combustion of firebrands. U.S. Department of Agriculture Forest Service Final Report of Grants FG-SP-114 and FG-SP-146. Madrid, May 1967.
47. Frössling, N., Über die verdunstung fallender tropfen. *Gerlands Beitr. Geophys.*, **52** (1938) 170–216.
48. Ohlemiller, T. J., Smoldering Combustion Propagation on Solid Wood. Center for Fire Research, National Institute of Standards and Technology (unpublished).
49. Atreya, A., Pyrolysis, ignition, and fire spread on horizontal surfaces of wood. Ph.D. Thesis, Harvard University, Cambridge, 1983.
50. Incropera, F. P. & DeWitt, D. P., Fundamentals of Heat and Mass Transfer, 3rd edn. John Wiley, New York, 1990; A15.
51. White, E. L. & Ward, J. J., Ignition of Metals in Oxygen, Report DMIC-224. Battelle Memorial Institute, 1966.
52. Clark, A. F. & Hust, J. G., A review of the compatibility of structural materials with oxygen. *AIAA Journal*, **12**(4) (1958) 663–72.
53. Emsley, J., The Elements, 3rd edn. Oxford University Press, Oxford, U.K., 1996.
54. Siegel, R. & Howell, J. R., Thermal Radiation Heat Transfer, 3rd edn. Hemisphere, Washington, 1992.